Nanoscale

# Spring-assisted hybrid triboelectric-electromagnetic nanogenerator for harvesting low-frequency vibration energy and creating self-powered security system



| | |
|---|---|
| Journal: | *Nanoscale* |
| Manuscript ID | NR-ART-05-2018-004276.R1 |
| Article Type: | Paper |
| Date Submitted by the Author: | 04-Jul-2018 |





| | |
|---|---|
| Complete List of Authors: | Wang, Weichao; Henan University<br>Xu, Jiancheng; Henan University<br>Zheng, H.W.; Henan University,<br>Chen, Fangqi ; Henan University<br>Jenkins, Kory; University of Minnesota, Mechanical Engineering<br>Wu, Yonghui; Henan University<br>Wang, Heyi; Henan University<br>Zhang, Weifeng; Henan University<br>Yang, Rusen; Xidian University |

# Spring-assisted hybrid triboelectric-electromagnetic nanogenerator for harvesting low-frequency vibration energy and creating self-powered security system

Weichao Wang,[†a] Jiancheng Xu,[†a] Haiwu Zheng,*[a] Fangqi Chen,[a] Kory Jenkins,[c] Yonghui Wu,[a] Heyi Wang,[a] Weifeng Zhang,*[a] and Rusen Yang *[b, c]

[a.] *Henan Key Laboratory of Photovoltaic Materials, School of Physics and Electronics, Henan University, Kaifeng 475004, China. E-mail: zhenghaiw@ustc.edu; wfzhang@163.com*

[b.] *School of Advanced Materials and Nanotechnology, Xidian University, Xi'an 710126, China. E-mail: rsyang@xidian.edu.cn*

[c.] *Department of Mechanical Engineering, University of Minnesota, Minneapolis, Minnesota 55455, USA.*

[†] W. C. Wang and J. C. Xu contributed equally to this work.

Electronic supplementary information (ESI) available.

**Abstract**

With the rapid development of portable electronics, exploring sustainable power sources is becoming more and more urgent. Utilizing a nanogenerator to harvest ambient mechanical energy could be an effective approach to solve this challenge. In this work, a novel spring-assisted hybrid nanogenerator (HG) consisting of a triboelectric nanogenerator (TENG) and an electromagnetic generator (EMG) was developed for harvesting low-frequency vibration energy. The results show that TENG with PTFE surface nanostructure has better output performance than that without the nanostructure. The effect of operation frequency on the open-circuit voltage and short-circuit current of the TENG and EMG is systematically investigated. Under a 2 Hz operating frequency, the EMG and TENG are able to produce a peak power of about 57.6 mW with a resistive load of 2000 Ω and 1682 $\mu$W with a resistive load of 50 MΩ, respectively. The impedance matching between TENG and EMG can be realized by using transformer to reduce the impedance of TENG. The charging performance of the HG is much better than that of the individual EMG or TENG. The HG enabled us to develop a self-powered safety system and to power LEDs, and drive some electronic devices. The present work provides a superior solution to improve the output performance of HG for harvesting low-frequency vibration energy.

## Introduction

With the increasing threats of fuel shortages, energy crises and environmental pollution, scavenging new and green energy sources from our natural environment has attracted considerable interest[1,2]. Mechanical energy is widely available from many sources in the environment, and can be harvested at many scales. There are many principles that can be utilized to turn mechanical energy into electrical energy, including electromagnetic induction[3,4], the electrostatic effect[5,6] and the piezoelectric effect[7-11]. EMGs have long been used for power generation because of their excellent stability and high output power, which has the characteristic of small output impedance with high current but low voltage. In brief, nanogenerators are the devices that generate electricity from the change of dielectric polarization caused by surface electrostatic charges, whether or not nanomaterials are employed[12,13]. When the surface charge comes from triboelectric effect, the nanogenerator can be defined as triboelectric nanogenerator (TENG). Although nanoscale materials are not essential, it has been reported that surface nanostructures of friction layer in TENG favor the improvement of output performance[14-18]. TENG based on the coupling of the triboelectric effect and electrostatic induction is a newly discovered method for harvesting mechanical energy, such as wind power[19-21], wave power[22-24], water power[25-27], and human motion power[28-31]. TENG have attracted great attention because of their high output energy and conversion efficiency, ease of manufacture, simple design and low material cost[32-34]. Compared with electromagnetic generator (EMG), TENG has large output impedance and produces high voltage but low current.

It is expected that a hybridization of TENG and EMG could take advantage of the complimentary output characteristics of each type of generator. The hybridization

of two separate energy harvesting modes means that more electrical energy can be extracted from one mechanical movement, improving the ability to power a variety of devices. Spring structures are commonly used for TENGs which harvest mechanical motion using contact-separation mode[35,36]. Spring-assisted hybrid nanogenerator (HG) composed of TENG and EMG components have been developed for harvesting mechanical energy, however, for a spring-assisted hybrid nanogenerator using vertical contact-separation motion, it can't ensure that the two friction surfaces of TENG are in full contact with each other. Moreover, the output of the HG is obviously reduced when the vibration amplitude of spring is smaller[37,38]. For the HG composed of TENG and EMG, the magnet generally move outside the coil or the coil turns in a fixed magnetic field, therefore, it is not easy to maximize the variation of magnetic flux in the coil so as to improve the output of EMG[37-39]. Hu et al. have reported a HG composed of TENG and EMG by using the principle of repulsion in the same polarity between two magnets, but its work frequency is above 2 Hz[40]. Zhang et al. have designed a novel HG as in-plane energy harvester, whose output power is still low[41]. To effectively capture low frequency vibration energy, further investigation of advanced structural design and device performance characterization are still needed.

In this paper, we report a spring-assisted HG with a novel structure that includes a TENG and an EMG, which were placed in the middle of the spring to form a body. The sliding mode of the TENG is used to ensure the two energy harvesting units can simultaneously scavenge low frequency energy, regardless of the vibration magnitude of the spring. The TENG consists of three concentric tubes, which effectively increases the friction area and improves the output performance of the nanogenerator for a given device volume. The EMG structure is designed to maximize the variation of magnetic flux in the copper coil, favoring the electrical output of the EMG. The

open-circuit voltage ($V_{oc}$) and short-circuit current ($I_{sc}$) of the TENG with three concentric tubes is 632 V and 12.2 $\mu$A, respectively, and the largest output power was 1682 $\mu$W (power per unit volume: 17.16 $\mu$W/cm$^3$) at a frequency of 2.0 Hz, which can directly light up 40 green commercial light-emitting diodes (LEDs) in series. Under the same mechanical motions, the EMG portion of the device produced a $V_{oc}$ of about 5.4 V, and an $I_{sc}$ of 36 mA. The maximum power produced by the EMG was 57.6 mW (power per unit volume: 2.35 mW/cm$^3$), which can directly light up forty LEDs in parallel. The total electrical energy produced by the HG can be stored in a capacitor or continuously power a digital temperature-humidity meter (DTHM), a liquid crystal display (LCD) with a complex picture, and a wireless alarm system for a bicycle. Furthermore, the current in the copper coils and in the spring of the HG will generate a new magnetic field, which will create a force that counteracts the movement of the device. This counteracting force can slow down the movement of the spring, thereby generating a dynamic damping effect to protect the electronic devices and equipment from shock damage.

## Experimental Section

### Fabrication of the spring-assisted HG

First, two commercially available cylinders of aluminum alloy were prepared with diameters of 5 cm and heights of 5.5 cm. One of the cylinders was machined into three connected concentric tubes with diameters of 4, 3.2 and 1.2 cm, respectively, all with a length of 5 cm and a wall thickness of 0.1 cm. The other cylinder was machined into two connected-concentric tubes with diameters of 3.6 and 2.8 cm, each with a length of 5 cm and a wall thickness of 0.1 cm. Next, a cylinder made of Polytetrafluoroethylene (PTFE) with an outer diameter of 3.8 cm and length of 5 cm

was processed into three separate tubes with external diameters of 3.8, 3.4 and 3.0 cm, respectively. The PTFE cylinders had a length of 5 cm and a wall thickness of 0.1 cm. The three PTFE tubes worked as the friction layers and were embedded into the aluminum alloy tubes. The aluminum tube with outside diameter of 3.6 cm serves as one electrode of the TENG, while the aluminum tube with an outside diameter of 4.0 cm serves as both a friction layer and other electrode of the TENG. The copper coils were fixed to the aluminum tube with an outer diameter of 1.2 cm, and the magnet rod was placed in the center of the aluminum tube with an outer diameter of 4.0 cm. The two terminals of the copper coil were used as the two electrodes of the EMG. Finally, a spring with an outer diameter of 5 cm and a length of 9 cm was fixed to the two interlocking aluminum tubes using hot glue.

**Fabrication of Nanostructure on PTFE Surface**

The PTFE with nanostructures was fabricated by using inductively coupled plasma (ICP) etching. First, PTFE tube was cleaned with acetone, ethyl alcohol, and DI water, respectively, and then blown dry by compressed nitrogen gas. Second, including the PTFE tube with a flexible mask, the exposed PTFE surface was treated with one power source of 400 W to produce a density of plasma, and another 100 W was used to accelerate the plasma ions for 30 seconds, while Ar, $O_2$, and $CF_4$ gases were introduced at flow rates of 15.0, 10.0, and 30.0 sccm, respectively. Finally, the surface of the PTFE will produce particle-like nanostructures because of ICP reactive ion etching. The surface morphology of the outer wall of the PTFE tube was characterized by field emission scanning electron microscopy (SEM, JSM-7001F).

**Electrical measurement of the HG**

The open-circuit voltages, short-circuit currents and short-circuit transferred charges of the devices were measured by a Keithley 6514 system electrometer. The HG was driven by a linear motor and its output performance was measured at different operation frequencies. The measurement software platform was made by LabVIEW, which is capable of enforcing real-time data acquisition control and analysis.

## Results and Discussion

### Structural design and working principle

Fig. 1a and d shows a schematic diagram and a photo of the HG, respectively. A complete drawing of the assembled HG is shown in Fig. 1b. Fig. 1c indicates SEM image of the outer wall of the PTFE tube with the surface nanostructures. The SEM image of the PTFE without surface nanostructures is shown in Fig. S1. The TENG operates in sliding mode by the relative displacement between the PTFE and the aluminum alloy tubes. This unique structure design enables the copper coils to cut magnetic lines more fully, resulting in a relatively large variation of magnetic flux in the coils and thus good electrical output from the EMG.

The cutaway drawing in Fig. 1e illustrates the electricity generation mechanisms of the TENG-EMG hybrid nanogenerator. These mechanisms are magnetic flux for the EMG, and short-circuit current and charge distribution for TENG. The initial state (Fig. 1e-i), the intermediate state (Fig. 1e-ii) and the final state (Fig. 1e-iii) are defined by the relative displacements between the two halves of the device (tube A and B) as the spring moves up and down. At the initial, intermediate, and final state, there is no overlap, some overlap and complete contact, respectively. The intermediate state is defined as the transitional process when tube A and tube B experiences apparent relative displacement. Likewise, the tube B in the initial and final states are wholly

misaligned and aligned with the tube A, respectively. At the intermediate state, the aluminum alloy with positive triboelectric charges is displaced relative to the PTFE which has negative triboelectric charges. Meanwhile, the magnetic flux crossing the copper coil will be enhanced when the magnet moves from the initial state to the intermediate state, resulting in an inductive electromotive force in the copper coils. In light of the Lenz's law, the induced current in the copper coils will generate a new magnetic field, which can hinder the increase in magnetic flux across the coil. Similarly, the transition from the intermediate state to the final state induces a current flowing in the same direction as that from the initial state to the intermediate state for both the TENG and the EMG. In contrast, the transition between the final state and the next initial state induces a current flow in the opposite direction for both the TENG and the EMG.

**Output performance of the HG**

To characterize the hybrid device for ambient mechanical energy harvesting, the output performance of both the TENG and EMG were measured and analyzed using a programmable linear motor. Tube B of the HG was directly mounted on the linear motor, and the moving distance of the motor was fixed. Fig. 2a-d provides a clear quantitative comparison of the electrical outputs of the TENG with and without the surface nanostructures of PTFE at different operation frequencies. As shown in Fig. 2a and 2b, the peak value of the $V_{oc}$ and $I_{sc}$ for the TENG without the nanostructures increases from ~ 323 to ~ 396 V and from ~ 1.7 to ~ 6.7 $\mu$A, respectively, with operation frequencies increasing from 0.4 to 2.0 Hz. As shown in Fig. 2c and 2d, the peak value of the $V_{oc}$ and $I_{sc}$ for the TENG with the nanostructures increases from ~ 536 to ~ 632 V and from ~ 3.5 to ~12.2 $\mu$A under the same operation conditions,

indicating the $V_{oc}$ and $I_{sc}$ of TENG with the nanostructures enhanced by almost two-folds compared to the TENG without the nanostructures. This is due to that the surface nanostructures of PTFE will bend when the device vibrates, the bending deformation and sliding movement of the nanostructures can improve the surface charge density of contact electrification by increasing the surface area between the sidewall of bent nanostructures and the opposite electrode[42,43], as seen from Fig. S2 and S3 at the frequency of 2 Hz. Thus, the output performance of the TENG enhanced with increasing surface charge density[44,45].

The effect of operation frequency on the open-circuit voltage and short-circuit current of the TENG with the nanostructures and the EMG is systematically further investigated. The $V_{oc}$ and $I_{sc}$ of the TENG operated at a frequency of 2.5 Hz are shown in Fig. S4. Further increasing the operating frequency from 2.0 to 2.5 Hz does not produce a significant increase in voltage. The $V_{oc}$ has a small increase from approximately 536 to 632 V with the rising frequency, which is consistent with the theoretical expectation that $V_{oc}$ is mainly determined by the displacement. The variation of $V_{oc}$ with respect to operation frequency in this case (Fig. S5a) is similar to that reported in the literature[16,46]. The dependence of short circuit transferred charges on frequency is shown in Fig. S3. It is clear that the transferred charge has a slight increase from 250 to 280 nC with the increasing frequency.

The $I_{sc}$ for the TENG increased with increasing frequency from 0.4 to 2.5 Hz, and unlike $V_{oc}$, continued to increase from 12.2 to 13.6 $\mu$A when the frequency increased from 2 to 2.5 Hz. A higher frequency is easily to bring about faster rates of contact and separation of the friction surfaces and could induce more transferred charges for a given time period compared with a lower frequency. From previous studies[47,48], the *I*-*Q* relationship for the TENG can be given by the following equation:

$$I_{sc}^{TENG} = \frac{dQ_{sc}}{dt} = \sigma \frac{dS(x)}{dt} \quad (1)$$

Where $Q_{sc}$ is the amount of short-circuit transferred charge, $x$, σ, and $S$ are sliding displacement, the surface charge density and the contact area of the two triboelectric layers, respectively. According to this equation, the $I_{sc}$ is nearly proportional to sliding speed and has been demonstrated to enhance linearly with the increase of frequency, which is in line with our experimental results (Fig. S5b). The vibration frequency of the spring in the HG is calculated to be about 10.4 Hz and the detailed calculation process can be seen in Supporting Information. The dependence of the $V_{oc}$ and $I_{sc}$ of the TENG on frequency is reasonable since the operating frequency is far below the resonance frequency.

Fig. 2e and 2f exhibit the open-circuit voltage and short-circuit current of the EMG under different operation frequencies, indicating that both the $V_{oc}$ and $I_{sc}$ increase with increasing operation frequency up to 2 Hz. The $V_{oc}$ and $I_{sc}$ of the EMG increase from ~ 0.8 to ~ 5.4 V and from ~ 1.2 to ~ 36 mA, respectively. On the basis of Faraday's law of electromagnetic induction, the relationship between open-circuit voltage and magnetic flux of the EMG can be expressed as

$$V_{oc}^{EMG} = -n \frac{d\Phi}{dt} \quad (2)$$

Where $n$ is the number of turns and $d\phi/dt$ is the change rate of magnetic flux in the copper coils. For the spring-assisted electromagnetic generator, the internal resistance $R$ of the copper coil is constant. The moving rate of the spring increases with increasing frequency during operation of the HG, resulting in faster movement speed of the magnetic rod in the copper coils. Therefore, the magnetic flux in the coils changed quickly, which leads to an increase of electromagnetic induction current. According to the Ohm's law, the current is proportional to the output voltage, so the output current of the EMG is also strongly related to the operation frequency and has

a similar variation trend as the output voltage. The dependence of $V_{oc}$ and $I_{sc}$ on the operation frequency of the EMG is indicated in Fig. S5c and S5d, from which an approximate linear relationship with the frequency can be observed, in accordance with Faraday's law.

To quantitatively study the output performance of the hybrid nanogenerator, the sliding displacement dependence of the output performance of both the TENG and EMG were measured and analyzed at the operation frequency of 2 Hz. As shown in Fig. 3a and 3b, the peak value of the $V_{oc}$ and $I_{sc}$ for the TENG increases from ~ 241 to ~ 632 V and from ~ 3.1 to ~12.2 $\mu$A, respectively, for sliding displacement increasing from 1.0 to 4.0 cm. From Fig. 3a and 3b, it is obvious the $V_{oc}$ and $I_{sc}$ of the TENG increases significantly with the increase of sliding displacement. Seen from Fig. 3c, it can be observed that the values of $V_{oc}$ and $I_{sc}$ have approximate linear relationship with the sliding displacement of the TENG. For the EMG part, the $V_{oc}$ and $I_{sc}$ of the EMG increase from ~ 1.52 to ~ 6.4 V and from ~ 9.2 to ~ 36 mA with the increase of sliding displacement ranging from 1 to 4 cm, respectively, as shown in Fig. 3d and 3e. The sliding displacement of the Tube A of the TENG also represents the motion distance of the magnet since and the magnet is fixed on Tube A. According to *Eq* 2 and the aforementioned analysis from Fig. 2d and 2e, the $V_{oc}$ and $I_{sc}$ of the EMG are proportional to the change rate of magnetic flux. For the current case, it is evident that the magnetic flux in the coil increases with the increase of the displacement distance of the magnet at the operation frequency of 2 Hz. Therefore, the $V_{oc}$ and $I_{sc}$ of the EMG increase with the increase of the sliding displacement. From Fig. 3f, it is demonstrated that the values of $V_{oc}$ and $I_{sc}$ of EMG enhance linearly with the increase of sliding displacement. From the above analysis, we can conclude that the sliding mode could ensure the two energy harvesting units scavenge low frequency energy

simultaneously in our hybrid device even at relatively low vibration magnitude of the spring. In other words, our novel HG worked in sliding mode has relatively large electrical output under low vibration magnitude, which is different from the spring-assisted hybrid nanogenerator worked in vertical contact-separation mode[37,38].

The output power of nanogenerator is maximized when they are connected to a matched external load. Consequently, the output performance of the TENG and EMG were evaluated separately with various load resistances at an operating frequency of 2 Hz. As reflected in Fig. 4a, as the external resistance load increases, the output voltage for the TENG increases and the output current decreases. The largest instantaneous peak power for the TENG reached 1682 $\mu$W with a volume power density of 17.16 $\mu$W/cm$^3$ at a loading resistance of 50 MΩ, as depicted in Fig. 4b. The maximum instantaneous peak power density for the TENG is comparable with other literatures[49,50]. The performance of the EMG was also estimated with different external resistance values. As illustrated in Fig. 4c, when the external loading resistance increases from 100 to 14000 Ω, the output voltage increases and the output current decreases significantly. The instantaneous output power is maximized when the external loading resistance is increased to 2000 Ω. The largest instantaneous power is 57.6 mW with a volume power density of 2.35 mW/cm$^3$, as presented in Fig. 4d. The output power of the EMG in this work is higher than other hybrid nanogenerator with EMG[51,52]. The power generation in the external spring was also investigated, and the $V_{oc}$ and $I_{sc}$ produced in the external spring reached 6.0 mV and 2.1 mA, respectively, when the operation frequency was 2.0 Hz, as manifested in Fig. S7. Furthermore, the short-circuit currents of the TENG and EMG were measured for 10000 cycles at the frequency of 1.0 Hz. As shown in Fig. 4e and 4f, almost no decline is observed for both the TENG and the EMG, which shows that the HG has

long-term stability.

As seen from Fig. 4b and 4d, the output impedance of TENG is far larger than that of EMG. To solve the problem of impedance matching between EMG and TENG, a transformer was used to obtain the low impedance of the TENG. As shown in Fig. 5a and 5b, a $V_{oc}$ of 5.3 V and $I_{sc}$ of 1.4 mA were produced for the TENG with the transformer. Fig. 5c shows the dependence of output voltage and current of the TENG on the external loading resistance with the transformer, the output voltage increases and the output current decreases with increasing loading resistance from 100 to 12000 Ω. The output impedance of the TENG was adjusted to 1 kΩ and the maximum instantaneous output power was 1.04 mW, as shown in Fig. 5d. Thus, the TENG could realize impedance matching with the EMG by a transformer, which corroborates the feasibility of direct connection of the TENG and EMG.

**Applications**

To demonstrate the capability of the HG as a sustainable power source, we used the nanogenerator to charge a capacitor and characterized the performance. As seen in Fig. 4a-d, the TENG delivers a low current output and a large voltage output, while the EMG obeys an opposite trend with a high current and low voltage. In order to effectively combine the electrical output from two types of generator, two full-wave bridge rectifiers connected in parallel were employed to electrically connect two generators. The circuit diagrams in Fig. 6a show how the nanogenerator was connected for practical applications including lighting LEDs, charging a capacitor, a

potential transformer (PT), powering a LCD and driving a DTHM. The voltage changes of the capacitor (10 $\mu$F) as charged by the TENG without transformer, EMG and combined HG (TENG without transformer//EMG) are plotted in Fig. 6b. Under a fixed charging time, the HG produces a higher charging voltage and faster charging rate than individual EMG and TENG that work separately, implying that the HG has much better charging performance than that of the individual energy-harvesting unit. In addition, it has been reported that the final charging level is determined by the output voltage, while the charging speed is decided by the output current[53]. As previously mentioned, the output characteristics for TENG and EMG are high voltage with low current and low voltage with high current, respectively. Therefore, it is not difficult to understand the fact that the voltage of the capacitor charged by TENG can obtain the maximum voltage with a long enough charging time. In marked contrast, the voltage of the capacitor charged by the EMG is restricted by the low open-circuit voltage of the EMG and saturation is achieved quickly in a relatively short charging time, resulting in the loss of the energy harvested. Taking advantage of both TENG and EMG, HG generates fast initial charging rate and provide high ultimate voltage. Moreover, the speed of charging a capacitor with a TENG can be further improved through either the power management system or the unique design of the charging cycle[54,55]. Fig. 6c shows the charging curves of the commercial capacitor (1000 $\mu$F) as charged by the TENG, TENG with a transformer, EMG, and the hybridized nanogenerator (TENG with a transformer//EMG). It is obvious that the TENG without the transformer has the lowest charging performance, the hybridized nanogenerator

has the better charging performance than that of each individual energy harvesting unit for a given time.

Commerciale LEDs were continuously powered by the HG. In our experiments, LEDs were divided into two groups. One group of 40 green LEDs (Fig. 6d-i) were connected to the TENG in series, assembling the word "HENU" and another group of green LEDs in series and red LEDs in parallel mixed circuit showing Xidian University in Chinese (Fig. 6d-ii). All the LEDs could be readily lit up by the HG when the device was pressed and released, as shown in Movies S2 and S3. To further prove the HG as a practical power source, three other applications were demonstrated. The HG was used to drive the DTHM and the LCD screen with a complex picture (LOGO of Henan University) with the aid of storage device, as seen in Fig. 6d-iii, Movie S4 and Fig. 6d-iv, Movie S5, respectively. Apart from these applications, the HG also has potential in the area of surveillance and security. For example, the spring-assisted hybrid nanogenerator was installed under a bicycle seat and connected to a wireless alarm system (Fig. 6d-v), which acted as a self-powered security sensor. The HG can easily drive a bicycle light for riding safely at night (Fig. 6d-vi). As the bicycle seat moves up and down, the electrical energy generated by the HG can drive the wireless alarm system and the white bike light, as demonstrated in Movie S6 and S7. The HG could also be used for similar applications in vehicles seat cushions with spring buffer structure. Furthermore, the HG along with the sensing system developed here has potential applications in diverse fields such as surveillance, remote operation and security systems.

It is well known that an energized wire is subjected to Ampere force in a magnetic field if the direction of current in the wire is not parallel to that of the magnetic field. Consequently, an Ampere force against motion of the spring was produced in the copper coil in our current configuration. This force has a tendency to resist spring motion and thus achieve the effect of vibration damping. Detailed calculation and derivation of the Ampere force in the copper coil is presented in the Supporting Information. Despite the difficulty in the measurement of the Ampere force and the weakness of vibration attenuation for the current device, a better vibration attenuation effect may be realized by increasing the magnetic field strength and turns of coils. These improvements are expected to expand the use of the HG to applications such as suspensions, shock absorber devices, and vibration control for mechanical equipment.

**Conclusions**

In summary, we have developed a TENG and EMG hybrid nanogenerator with unique structure design, which can generate electricity by capturing the mechanical energy simultaneously from one motion at low frequency (motion frequency ranging from 0.4 to 2.0 Hz). In this design, The TENG and EMG in the hybrid device are driven by the elastic restoring force of the spring. Furthermore, the novel tube-like electrode of the TENG makes the output performance robust and durable. Meanwhile, the distinctive relative movement between the magnet and the coils maximizes the change in the magnetic flux in the copper coils, favoring the output performance of the EMG.

The TENG produces a $V_{oc}$ of about 632 V, and an $I_{sc}$ of 12.2 $\mu$A with a maximum output power of about 1682 $\mu$W and a volume power density of 17.16 $\mu$W/cm$^3$ at the frequency of 2.0 Hz. Under the same mechanical motions, the EMG can produce a $V_{oc}$ of about 5.4 V, and an $I_{sc}$ of 36 mA with a largest output power of 57.6 mW and a volume power density of 2.35 mW/cm$^3$, respectively. As compared with the TENG without transformer, the application of transformer reduces the impedance of TENG and obviously increases the charging rate. Compared with the individual energy-harvesting unit, the HG has much better charging performance and can be utilized to sustainably power electronics such as LEDs, a DTHM, and a LCD with complex picture. In addition, the spring-assisted HG has application potential in the areas of self-powered security alarm system and vibration attenuation. This work will render an effective and sustainable progress in low frequency mechanical energy harvesting techniques and practical applications for HG as power sources and self-powered devices.

**Conflicts of interest**

There are no conflicts to declare.

**Acknowledgements**

This work is supported by the NSFC (Nos. 51372069), Scientific and Technological Project in Henan Province (172102210013), Program for Innovative Research Team in Science and Technology in University of Henan Province (19IRTSTHN019). NSF (ECCS-1150147), NSF IGERT grant (DGE-1069104), Chongqing Research program of Basic Research and Frontier Technology (No.cstc2016jcyjA0236).

**Notes and references**


1 A. Khaligh, O. C. Onar, CRC Press, Boca Raton, FL, 2009.

2 Z. L. Wang, G. Zhu, Y. Yang, S. H. Wang, C. F. Pan, *Mater. Today,* 2012, **15**, 532.

3 R. Amirtharajah, A. P. Chandrakasan, *IEEE J. Solid-State Circ.,* 1998, **33**, 687.

4 C. B. Williams, R. B. Yates, *A: Phys*., 1996, **52**, 8.

5 S. Meninger, J. O. Mur-Miranda, R. Amirtharajah, A. P. Chandrakasan, J. H. Lang, I*EEE Trans. VLSI. Syst.,* 2001, **9**, 64.

6 S. Roundy, P. K. Wright, J. Rabaey, *Comput. Commun.,* 2003, **26**, 1131.

7 P. Glynne-Jones, S. P. Beeby, N. M. White, *IEE Proc.-Sci. Meas. Technol.,* 2001, **148**, 68.

8 S. Roundy, E. S. Leland, J. Baker, E. Carleton, E. Reilly, B. Otis, J. M. Rabaey, P. K. Wright, V. Sundararajan, *IEEE Pervas. Comput.,* 2005, **4**, 28.

9 Z. L. Wang, J. H. Song, *Science*, 2006, **312**, 242.

10 X. Han, M. X. Chen, C. F. Pan, Z. L. Wang, *J. Mater. Chem. C.,* 2017, **4**, 11341.

11 R. A. Whiter, V. Narayan, K-N. Sohini, *Adv. Energy. Mater.,* 2014, **4**, 1400519.

12 Z. L. Wang, *Mater. Today*, 2017, **20**, 74.

13 C. Zhang, W. Tang , C. B. Han, F. R. Fan, Z. L. Wang, *Adv. Mater*., 2014, **26**, 3580.

14 L. Lin, Y. N. Xie, S. M. Niu, S. H. Wang, P-K. Yang, Z. L. Wang, *ACS Nano*, 2015, **9**, 922.

15 H. J. Fang, Q. Li, W. H He, J, Li, Q. T. Xue, C. Xu, L. J. Zhang, T. L. Ren, G. F. Dong, H. L. W. Chan, J. Y. Dai, Q. F. Yan, *Nanoscale*, 2015, **7**, 17306.

16 S. H. Wang, L. Lin, Y. N, Xie, Q. S. Jing, S. M. Niu, Z. L. Wang, *Nano Lett.*, 2013, **13**, 2226.

17 H. Wang, M. Y. Shi, K. Zhu, Z. M. Su, X. L. Cheng, Y. Song, X. X. Chen, Z.Q. Liao, M. Zhang, H. X. Zhang, *Nanoscale*, 2016, 8, 18489.

18 C. Y. Wan, C. R. Bowen, *J. Mater. Chem. A*., 2017, **5**, 3091.

19 Z. Zhao, X. Pu, C. Du, L. Li, C. Jiang, W. Hu, Z. L. Wang, *ACS Nano*, 2016, **10**, 1780.

20 Y. Yang, G. Zhu, H. Zhang, J. Chen, X. Zhong, Z. H. Lin, Y. Su, P. Bai, X. Wen, Z. L. Wang, *ACS Nan*o, 2013, **7**, 9461.

21 H. Y. Guo, X. M. He, J. W. Zhong, Q. Z. Zhong, Q. Leng, C. G Hu, J. Chen, L. Tian, Y. Xia, J. Zhou, *J. Mater. Chem. A.,* 2014, **2**, 2079.

22 Y. Su, X. Wen, G. Zhu, J. Yang, J. Chen, P. Bai, Z. Wu, Y. Jiang, Z. L. Wang, *Nano Energy*, 2014, **9**, 186.

23 G. Zhu, Y. Su, P. Bai, J. Chen, Q. Jing, W. Yang, Z. L. Wang, *ACS Nano*, 2014, **8**, 6031.

24 T. Jiang, L. M. Zhang, X. Chen, C. B. Han, W. Tang, C. Zhang, L. Xu, Z. L. Wang, *ACS Nano*, 2015, **9**, 12562.

25 Q. Liang, X. Yan, Y. Gu, K. Zhang, M. Liang, S. Lu, X. Zheng, Y. Zhang, *Sci. Rep.,* 2015, **5**, 9080.

26 S-B. Jeon, D. Kim, G-W. Yoon, J-B. Yoon, Y-K. Choi, *Nano Energy,* 2015, **12**, 636.

27 Z-H. Lin, G. Cheng, S. Lee, K. C. Pradel, Z. L. Wang, *Adv. Mater.,* 2014, **26**,

4690.

28 Y, L. Zi, H. Y. Guo, Z. Wen, M.-H. Yeh, C. G. Hu, Z. L. Wang, *ACS Nano*, 2016, **10**, 4797.

29 A. Chinnappan, C. Baskar, S. Baskar,G. Ratheesh and S. Ramakrishna, *J. Mater. Chem. C.,* 2017, **5**, 12657.

30 J. Chung, W. Kim, W. J. Jang, H-W. Park, A. Sohn, K-B. Chung, D-W. Kim, D. Choi, Y. T. Park. *J. Mater. Chem. A.,* 2018, **6**, 3108.

31 X. J. Pu, H. Y. Guo, J. Chen, X. Wang, Y. Xi, C. G. Hu, Z. L. Wang, *Sci. Adv*., 2017, **3**, e1700694.

32 L. McCarty, G. Whitesides, *Angew. Chem. Int. Ed.,* 2008, **47**, 2188.

33 Z. L. Wang, *ACS Nano*, 2013, **7**, 9533.

34 G. L. Liu, J. Chen, Q. Tang, L. Feng, H. M. Yang, J. Li, Y. Xi, X. Wang, C. G. Hu, *Adv. Energy. Mater.*, 2018, **8**, 1703086.

35 T. Jiang, Y. Y. Yao, L. Xu, L. M. Zhang, T. X, Xiao, Z. L. Wang, *Nano Energy*, 2017, **31**, 560.

36 C. S. Wu, R. Y. Liu, J. Wang, Y. L. Zia, L. Lin, Z. L. Wang, *Nano Energy*, 2017, **32**, 287.

37 T. Quan, Y. C. Wu, Y. Yang, *Nano Research*, 2015, **10**, 3272.

38 K. W. Zhang, X. Wang, Y. Yang, Z. L. Wang, *ACS Nano,* 2015, **9**, 3521.

36 39 K. W. Zhang, Z. L. Wang, Y. Yang, *ACS Nano*, 2016, **10**, 4728.

40 Y. F. Hu, J. Yang, S. M. Niu, W. Z. Wu, Z. L. Wang, *ACS Nano*, 2014, **8**, 7442.

41 X. X. Chena, H. Guo, H. X. Wu, H. T. Chen, Y. Song, Z. M. Su, H. X. Zhang,

*Nano Energy*, 2018, **49**, 51.

42 X. M. Li, C. Xu, C. Wang, J. Y. Shao, X. L. Chen, C. H. Wang, H. M. Tian, Y. Wang, Q. Z, Yang, L. Wang, B. H. Lu, *Nano Energy*, 2017, **40**, 646.

43 S. H. Wang, L. Lin, Z. L. Wang, *Nano Lett.*, 2012, **12**, 6339.

44 B. U. Ye, S. Y. Lee, M. Jung, S-D. Sohn, H-J. Shin, M. H. Song, K. J. Choi, J. M. Baik, *Nanoscale*, 2017, **9**, 18597.

45 Y. L. Zi, S. M. Niu, J. Wang, Z. Wen, W. Tang, Z. L. Wang, *Nat. Commun*., 2015, **6**, 8376.

46 B. B. Zhang, J. Chen, L. Jin, W. L. Deng, L. Zhang, H. T. Zhang, M. H. Zhu, W. Q. Yang, Z. L. Wang, *ACS Nano*., 2016, **6**, 6241.

47 S. M. Niu, Y. Liu, S. H. Wang, L. Lin, Y. S. Zhou, Y. F. Hu, Z. L. Wang, *Adv. Mater.,* 2013, **25**, 6184.

48 L. Chen, H. Y. Guo, X, N. Xia, G, L, Liu, H, F. Shi, M. J. Wang, Y. Xi, C. G. Hu, *ACS Appl. Mater. Interfaces.,* 2015, **7**, 16450.

49 Y. C. Wu, X. Wang, Y. Yang, Z. L. Wang, *Nano Energy*., 2015, **11**, 162.

50 X. M. Lia, C. Xu, C. Wang, J. Y. Shao, X. L. Chen, C. H. Wang, H. M. Tian, Y. Wang, Q. Z. Yang, L. Wang, B. H. Lu, *Nano Energy*., 2017, **40**, 646.

51 K. W. Zhang, Y. Yang, *Nano Research*., 2016, **9**, 974.

52 X. Wang, Z. L. Wang, Y. Yang, *Nano Energy*., 2016, **26**, 164.

53 X. Wang, Z. Wen, H. Y. Guo, C. S. Wu, X. He, L. Lin, X. Cao, Z. L. Wang, *ACS Nano*., 2016, **10**, 11369.

54 S. Niu, X. Wang, F. Yi, Y. Zhou, Z. L. Wang, *Nat. Commun*., 2015, **6**, 8975.

55 Y. L. Zi, J. Wang, S. H. Wang, S. Li, Z. Wen, H. Y. Guo, Z. L. Wang, *Nat. Commun.*, 2016, **7**, 10987.

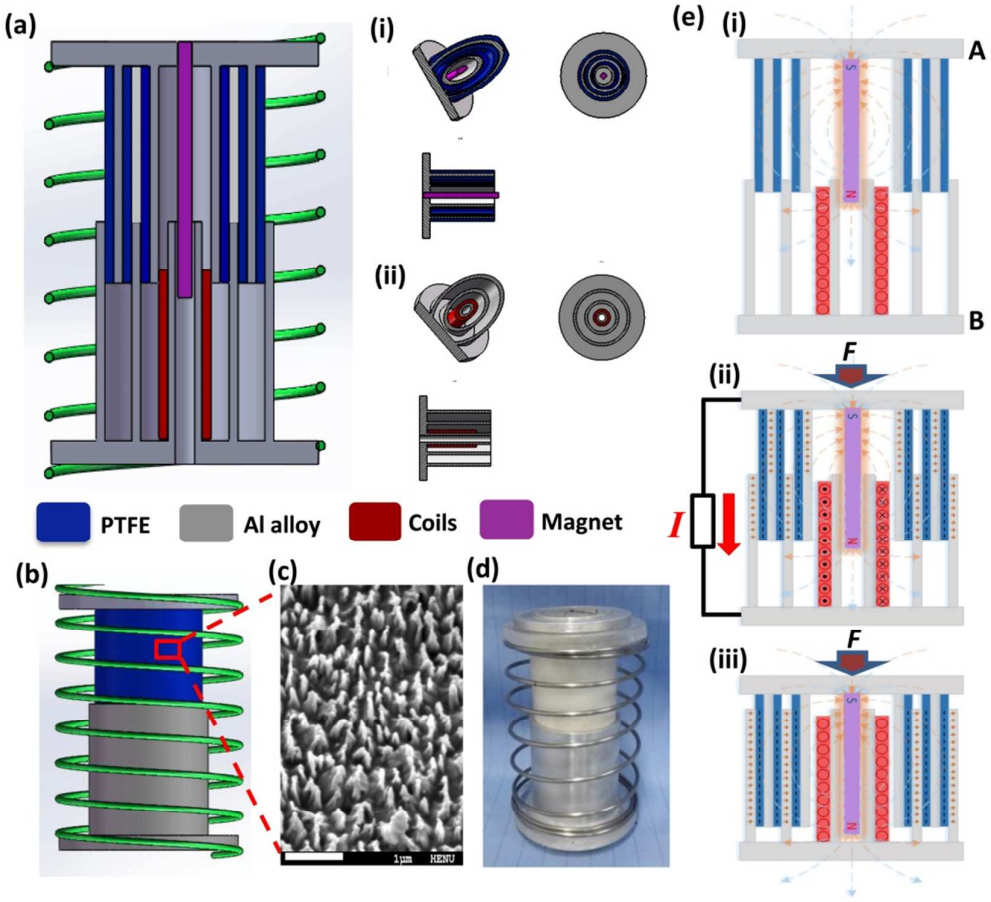


**Fig. 1** Structural design and working principle of a HG. (a) Sectional view of a HG composed of TENG and EMG. (i) and (ii) the two components of the hybrid nanogenerator. (b) Drawing of the spring-assisted HG. (c) The SEM images of the PTFE tube showing nanostructures. (d) Photograph of the HG. (e) Magnetic fields, charges distribution and current flow in the device during the initial state (i), intermediate state (ii) and final state (iii).

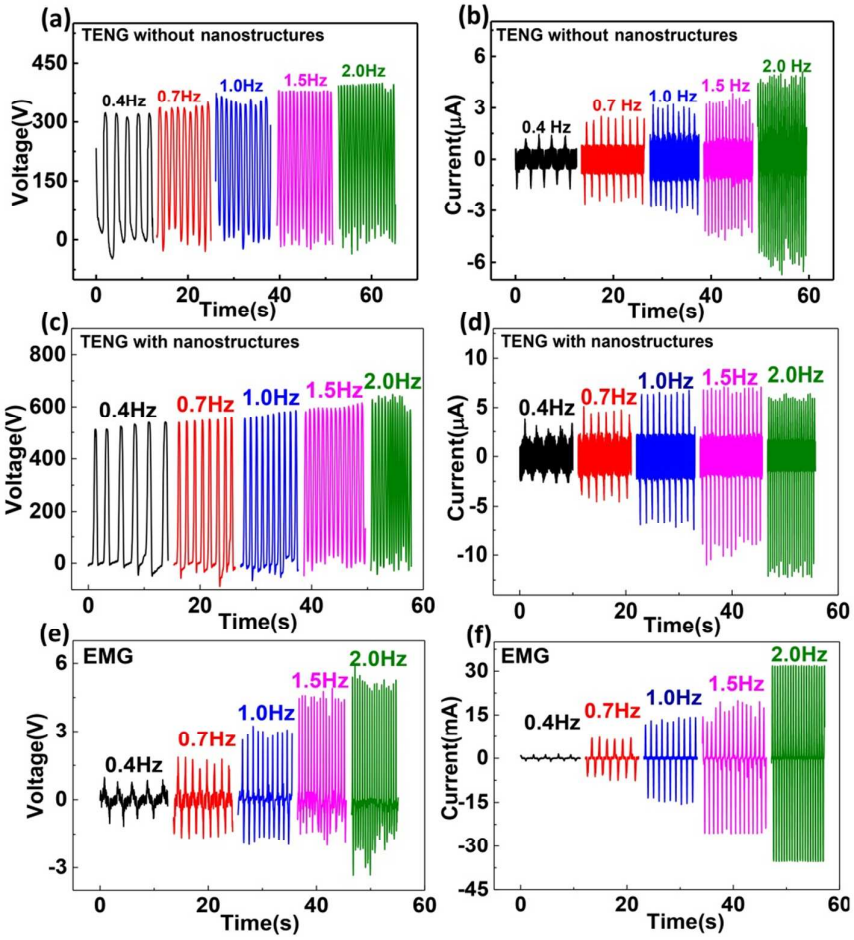


**Fig. 2** Electrical output performances of a HG under different operation frequencies. The open-circuit voltage (a, c) and the short-circuit current (b, d) of the TENG without and with the surface nanostructures of PTFE, respectively. The $V_{oc}$ (e) and $I_{sc}$ (f) of EMG.

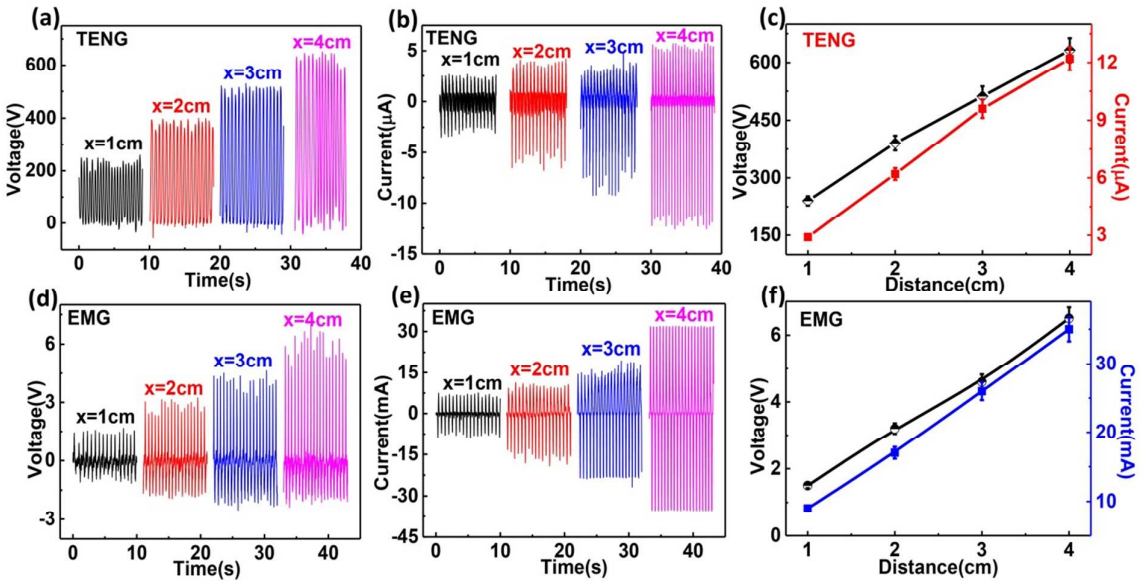


**Fig. 3** Output voltage and current of TENG (a, b) and EMG (d, e) at the frequency of 2 Hz and different sliding displacement *x*. The dependence of the $V_{oc}$ and $I_{sc}$ of the TENG (c) and EMG (f) on sliding displacement ranging from 1.0 to 4.0 cm.

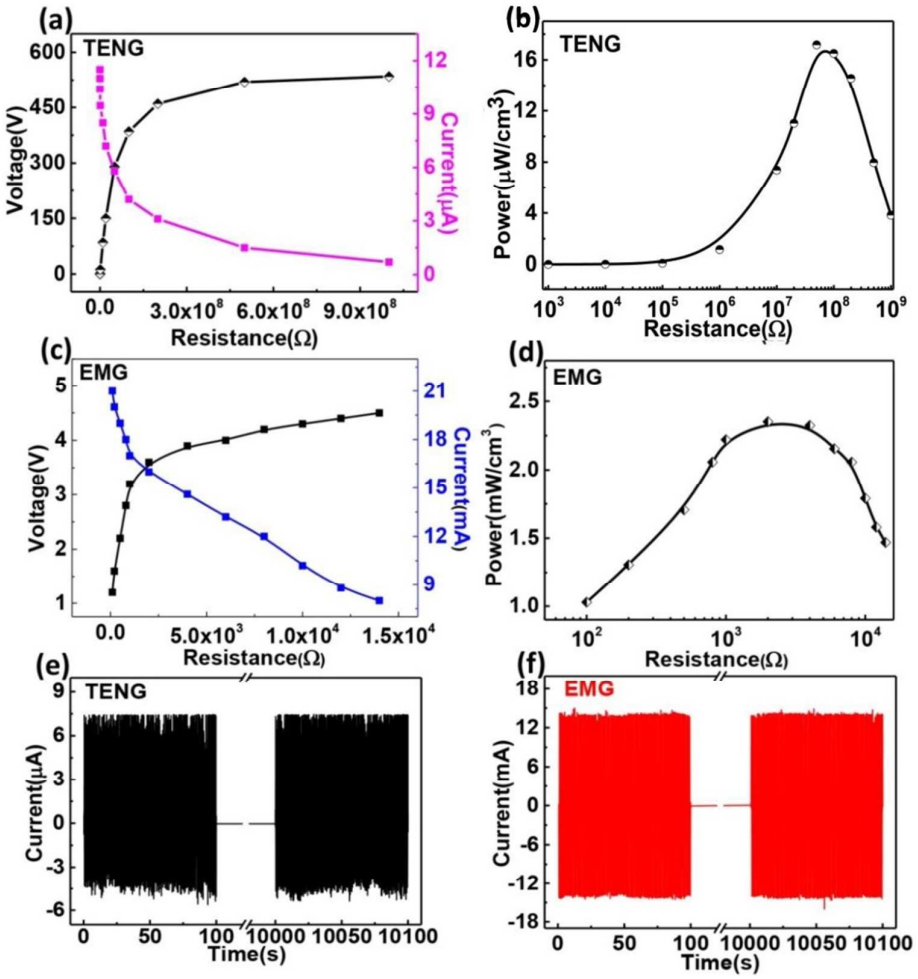


**Fig. 4** Output power performances of TENG and EMG at the frequency of 2Hz. Output voltage and output current of TENG (a) and EMG (c) at different external resistance loads. The dependence of the instantaneous power densities of TENG (b) and EMG (d) on the external load resistances. Short-circuit current of the TENG (e) and EMG (f) was measured for 10000 cycles at a frequency of 1 Hz.

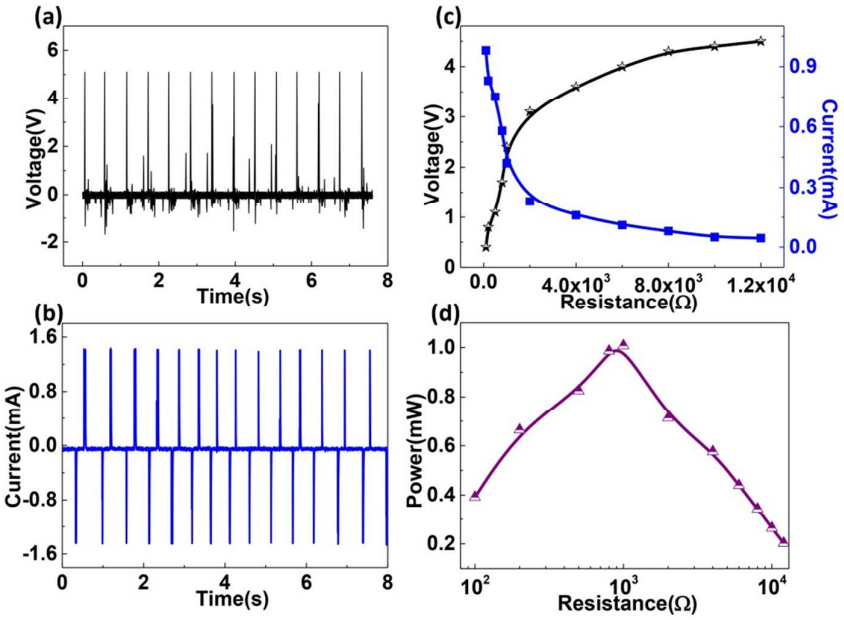


**Fig. 5** Output performances of the TENG with a transformer. Open-circuit voltage (a) and short-circuit current (b) of the TENG. Dependence of output current and voltage (c) and output power (d) of the TENG with a transformer on the external loading resistance.

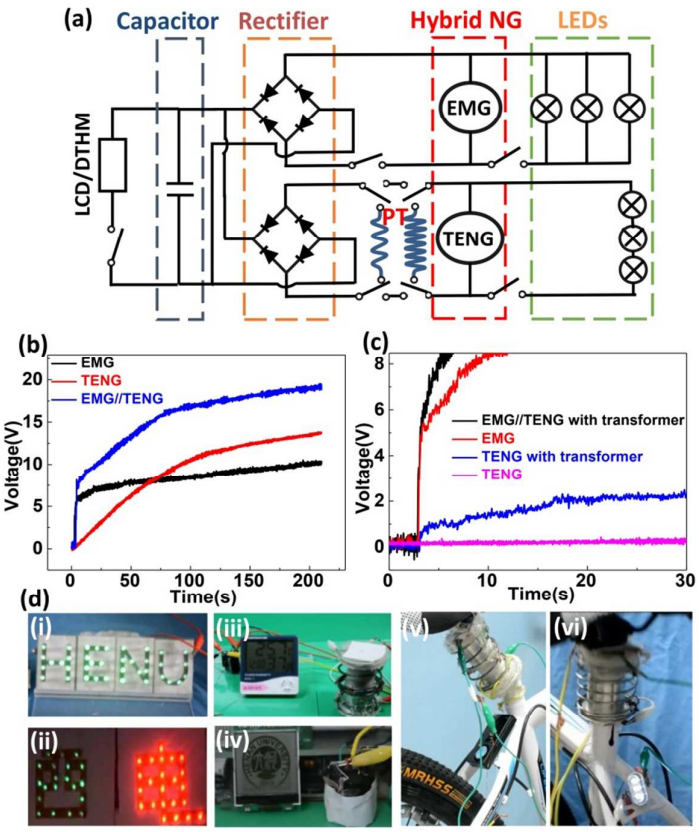


**Fig. 6** Demonstration of the packaged HG as a practical power source. (a) The circuit diagram for lighting LEDs, charging capacitors and powering LCD/DTHM. (b)The charging curves of a 10 $\mu$F capacitor using EMG only, TENG only, and hybrid nanogenerator, respectively. (c) Measured voltage of a 1000 $\mu$F capacitor charged by the TENG, EMG, TENG with a transformer, and the hybridized nanogenerator (EMG and TENG with a transformer in parallel). (d) Photographs of the HG acting as a power sources to drive. (i) 40 green LEDs in series showing the word "HENU", (ii) mixed circuit of "西" green LEDs in series and "电" red LEDs in parallel showing Xidian University in Chinese, (iii) a monitor showing the time, temperature, and humidity. (iv) LOGO of Henan University, (v) a wireless alarm system under the bicycle seat, and (vi) bicycle warning safety light.